analytical chemistry

Article

pubs.acs.org/ac

Proximity Hybridization Regulated DNA Biogate for Sensitive Electrochemical Immunoassay

Kewei Ren,[†,§] Jie Wu,[†,§] Yue Zhang,[†] Feng Yan,[‡] and Huangxian Ju*[,†]

[†]State Key Laboratory of Analytical Chemistry for Life Science, School of Chemistry and Chemical Engineering, Nanjing University, Nanjing 210093, China

[‡]Department of Clinical Laboratory, Nanjing Medical University Cancer Hospital & Jiangsu Cancer Hospital, Nanjing 210009, China

Supporting Information

ABSTRACT: An electrochemical DNA biogate was designed for highly sensitive homogeneous electrochemical immunoassay by combining target-induced proximity hybridization with a mesoporous silica nanoprobe (MSN). The electroactive methylene blue (MB) was sealed in the inner pores of MSN with single-stranded DNA. In the presence of target protein and two DNA-labeled antibodies, the formed proximate complex could hybridize with the DNA strand to form a rigid double-stranded structure and thus open the biogate, which led to the release of MB entrapped in the MSN. The target protein-dependent amount of released MB could be conveniently monitored with a screen-printed carbon electrode. Moreover, the detachment process of MB could be further amplified with an in situ enzymatic recycling binding of the proximate complex with the single-stranded DNA. Using prostate-specific antigen as a model target, the proposed assay showed a wide detection range from 0.002 to 100 ng mL^{-1} with a detection limit of 1.3 pg mL^{-1}. This strategy was simple and universal for various analytes with different affinity ligands. This method possessed great potential for convenient point-of-care testing and commercial application.

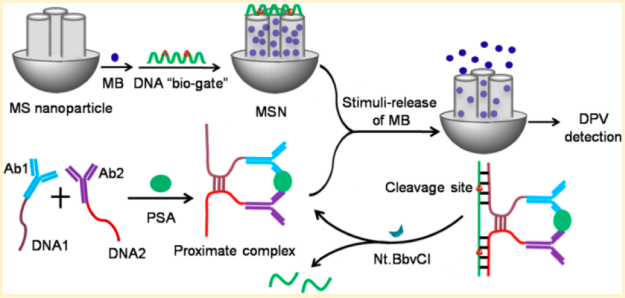

Great advances in nanoscience have provided exciting technologies and novel materials for the bioassay field due to the unique optical, magnetic, mechanical, chemical, and physical properties of nanomaterials.[1] Various types of nanomaterials, such as carbon nanotubes,[2,3] magnetic beads,[4,5] gold nanoparticles,[6] and quantum dots,[7] have been applied to design highly sensitive methods for electrochemical immunoassays. The specific surface area and unique electrical conductivity of nanomaterials lead to their wide use in the design of trace nanoprobes and the construction of immunosensing interfaces. These nanomaterial-based electrochemical immunoassay methods generally exhibit a high ratio of signal-to-noise and high detection sensitivity. However, most of them are performed in heterogeneous systems and require wash and separation steps, which limit their application in common point-of-care testing.[8]

Homogeneous immunoassay is an attractive detection format because it reduces the risk of contamination, eliminates time-consuming operation steps, and is easy to design high-throughput and automation systems.[9] Therefore, some nanomaterials have been used for the construction of homogeneous fluorescent or colorimetric immunoassay methods via the resonance energy transfer or nanoparticle aggregation phenomena.[10−12] This work used mesoporous silica (MS) nanoparticles to design a DNA biogate for homogeneous electrochemical immunoassay.

MS nanoparticles contain hundreds of channels (mesopores) arranged in a 3D network of honeycomb-like porous structure.[13] Due to the unique pore structure, biocompatibility and ease of functionalization, MS nanoparticles have attracted substantial research attention in the fields of biotechnology and nanomedicine. Particularly, some signal molecules can be filled in the mesopores of MS nanoparticles and then sealed with different gatekeepers such as organic molecules, nanoparticles, supramolecules, and biomolecules[14−17] to construct stimuli-responsive MS nanoprobes (MSNs). Various stimuli, such as redox reagents,[18,19] pH,[20] enzymes,[21] and photoirradiation,[22,23] have been implemented to trigger the opening of the pores and controllable release of the encapsulated substrates. These stimuli-responsive MSNs are frequently used as delivery vehicles and sensory nanoprobes. For example, a fluorescent dye has been entrapped within a magnetic MSN for fluorescence immunoassay,[24] and the electroactive methylene blue (MB) has also been sealed in antibody-conjugated MSNs with aminated polystyrene microsphere through the electrostatic interaction.[25] The latter has been used for electrochemical immunoassay by using the specific immunoreaction to displace the microsphere and open the molecular gate for release of MB.

Received: April 5, 2014
Accepted: June 26, 2014
Published: June 26, 2014

   dx.doi.org/10.1021/ac5012377 | *Anal. Chem.* 2014, 86, 7494−7499

Scheme 1. Schematic Illustration of Homogeneous Electrochemical Immunoassay Using Proximity Hybridization-Responsive Mesoporous Silica Nanoprobe

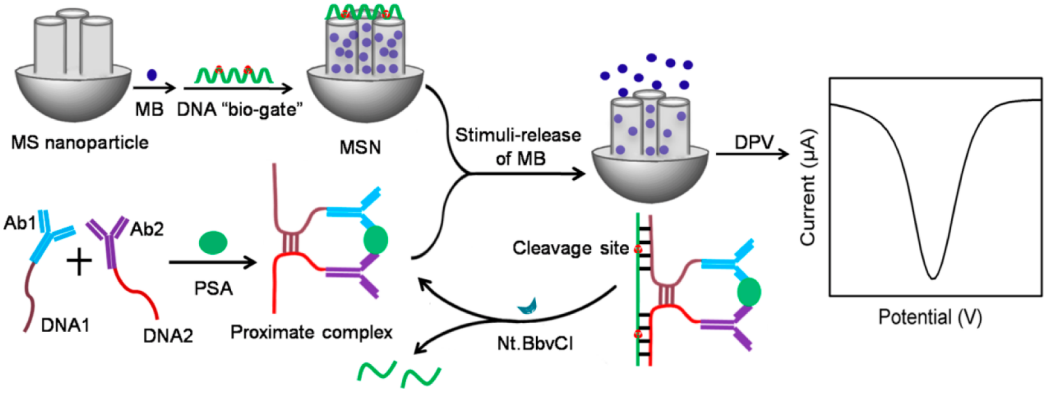

This work made use of the flexible binding properties of DNA[26] to seal MB in the mesopores, which excluded the steric hindrance of the immunocomplex formed on MSN to MB release and simplified the sealing procedure of MB. The DNA strand could conveniently detach from the MSN surface upon its hybridization with a complementary DNA strand.[27] Thus, the target-induced proximity hybridization[28−31] was introduced to form a proximate complex for the design of a regulated DNA biogate, which provided the complementary DNA strand by using two DNA strand-labeled antibodies to recognize the target protein (Scheme 1). More importantly, the in situ recycling of the proximate complex could be achieved with nicking endonuclease Nt.BbvCI to open more DNA biogates for release of more MB, thus amplifying the electrochemical signal. Under optimal conditions, the proposed homogeneous electrochemical immunoassay method could detect prostate-specific antigen (PSA) with a detection range of 4 orders of magnitude, along with a detection limit at pg mL^{-1} level. This strategy could be conveniently extended for a wide range of analytes with available affinity ligands to form the proximate complex and provided a novel protocol for point-of-care testing of protein markers.

EXPERIMENTAL SECTION

Reagents and Materials. *N*-Cetyltrimethylammonium bromide (CTABr), sulfosuccinimidyl-4-(*N*-maleimidomethyl)-cyclohexane-1-carboxylate (SMCC), and tetraethylorthosilicate (TEOS) were supplied by Heowns Biochem LLC (Tianjin, China). PSA and mouse monoclonal anti-PSA antibodies (clone no. P27B1 as Ab1 and P27A10 as Ab2) were purchased from Shuangliu Zhenglong Biochem Lab (Chengdu, China). MB and 3-aminopropyltriethoxysilane (APTES) were purchased from Sigma-Aldrich (USA). Nt.BbvCI (10 000 U mL^{-1}, one unit is defined as the amount of enzyme required to convert 1 μg of supercoiled plasmid DNA to open the circular form in 1 h at 37 °C in a total reaction volume of 50 μL) and 10× NEB buffer 4 were purchased from New England Biolabs (Ipswich, MA) and used without further purification. The clinical serum samples from prostate cancer patients were obtained from Jiangsu Institute of Cancer Prevention and Cure and stored at −20 °C before use. The serum samples were used directly without any treatment. DNA loading buffer (6×) was bought from Solarbio Co. Ltd. (Beijing, China). Low molecular DNA ladder was purchased from Fermentas. Ultrapure water obtained from a Millipore water purification system (≥18 MΩ, Milli-Q, Millipore) was used in all assays. Hybridization buffer (HB, pH 7.4) contained 10 mM Tris-HCl, 50 mM NaCl, and 10 mM $MgCl_2$. Dithiothreitol (DTT) and oligonucleotides were obtained from Sangon Biotechnology Inc. (Shanghai, China), and the oligonucleotide sequences were as follows:

DNA1: 5′-**GCTGAGGTT**AT***CAAGAC***TTTTTTTTA-TCACATCA***GGCTCTAGCGTATGCTATTG***-SH-3′

DNA2: 5′-SH-TACGTCCAGAACTTTACCAAA-CCACACCCTTTTTTT***GTCTTG***GCTGAGGAT-3′

DNA2′ (4 bp complementary with DNA1): 5′-*TACGTCCAGAACTTTACCAA*ACCACACCCTTTTTTTTA-***CTTG***GCTGAGGAT-3′

DNA2′ (6 bp complementary with DNA1): 5′-*TACGTCCAGAACTTTACCAAA*CCACACCCTTTTTTT-***GTCTTG***GCTGAGGAT-3′

DNA2′ (8 bp complementary with DNA1): 5′-*TACGTCCAGAACTTTACCAAACCA*CACACCCTTTTT-***AAGTCTTG***GCTGAGGAT-3′

DNA2′ (10 bp complementary with DNA1): 5′-*TACGTCCAGAACTTTACCAAACCACA*CACCCTTT-***AAAAGTCTTG***GCTGAGGAT-3′

ref DNA: 5′-*TTGGTAAAGTTCTGGACGTA-TCTCCCATTGTAGTATCTTGTAGTATCT-CCCATCACCAGTCAATAGCATACGCTAGAGCC*-3′

DNA3 for preparation of MSN: 5′-GTAATCC▲TCA-GCAACC▲TCAGC-3′

DNA3′: 5′-aminomethylcoumarin (AMCA)-GTAATCC▲TCAGCAACC▲TCAGC-3′

The binding regions between DNA3 or DNA3′ and DNA1 and DNA2 or DNA2′ are shown in bold and underlined, respectively; the binding region between DNA1 and DNA2 or DNA2′ is shown in bold and italics, and the binding region between ref DNA and DNA1 and DNA2′ is shown in italics. The cleavage sites for Nt.BbvCI are marked with "▲".

Apparatus. The electrochemical measurements were performed on a CHI 630D electrochemical workstation (CH Instruments Inc., USA) at room temperature with a portable homemade screen-printed electrode, which consists of a carbon working electrode (2 mm diameter), a carbon auxiliary electrode, and a Ag/AgCl reference electrode. The insulating layer printed around the working area constituted a reservoir of an electrochemical cell (7 mm diameter), and the relative standard deviation between electrodes is 3.32% (eight measurements). The transmission electron microscopic (TEM) images were obtained on a JEM-2100 transmission electron microscope (JEOL Ltd., Japan). Nitrogen absorption/desorption measurement was obtained with a porosimeter (ASAP 2020,

dx.doi.org/10.1021/ac5012377 | Anal. Chem. 2014, 86, 7494−7499

Micromeritics, USA). Dynamic light scattering (DLS) was observed on a 90 Plus/BI-MAS equipment (Brookhaven, USA). Zeta-potential analysis was performed on a Zetasizer (Nano-Z, Malvern, UK). The fluorescence spectra were obtained on a RF-5301PC spectrofluorophotometer (Shimadzu, Japan). The polyacrylamide gel electrophoresis was performed on the DYCP-31BN electrophoresis analyzer (Liuyi Instrument Company, China) and imaged on Biorad ChemDoc XRS (Bio-Rad, USA).

Preparation of MSN. The MS nanoparticles were first synthesized with the following procedure.[32] First, 1.75 mL of NaOH (2.00 M) was added to 240 mL of CTABr (2 mg mL^{-1}) and heated to 95 °C. Under continuous stirring, 2.5 mL of TEOS was added dropwise. The mixture was allowed stirring for 3 h to give a white precipitate. Then the solid product was centrifuged, washed with deionized water and ethanol, and dried at 60 °C overnight. The obtained white powder was finally calcined at 550 °C using oxidant atmosphere for 5 h to remove the template phase.

Next, 0.5 g of calcined MS nanoparticles and 0.5 mL of APTES were suspensed in 50 mL of anhydrous ethanol inside a round-bottom flask. After the mixture was stirred continuously for 6 h at 36 °C, it was filtered, washed with ethanol, and dried at 60 °C to obtain amine-functionalized MS nanoparticles. Then, 1 mg of amine-functionalized nanoparticles was dispersed in 1 mL of hybridization buffer containing 30 mg mL^{-1} MB. The mixture was shaken overnight in the dark at room temperature and then was centrifuged and washed with ultrapure water to obtain MB-loaded MS nanoparticles (MB-MS), which were further suspended in 1 mL of hybridization buffer containing 0.04 mM DNA3 and shaken for 60 min at room temperature. The resulting solids were isolated by centrifugation and washed with hybridization buffer to obtain MSN.

In order to optimize the amount of DNA used for sealing the MB in mesopores of MS nanoparticles, AMCA-labeled DNA (DNA3′) was used to replace DNA3 for preparation of control MSN. One hundred micrograms of MS nanoparticles was suspended in 100 μL of hybridization buffer containing 0.04 mM DNA3′ and shaken for 60 min at room temperature. The resulting nanoparticles were isolated by centrifugation and washed twice with 100 μL of hybridization buffer to eliminate the residual DNA3′. The amount of capped DNA3′ on MSN could be measured from the fluorescence intensity of the supernatant.

Preparation of DNA-Labeled Antibody. The DNA-labeled antibodies (Ab-DNA) were synthesized according to the previous work.[33] Briefly, anti-PSA antibody (2 mg mL^{-1}) was first reacted with a 20-fold molar excess of SMCC in PBS (55 mM phosphate, pH 7.4, 150 mM NaCl, 20 mM EDTA) for 2 h at room temperature. In parallel, 3 μL of 100 μM thiolated ssDNA was reduced with 4 μL of 100 mM DTT in PBS for 1 h at 37 °C. Both products were purified by ultrafiltration (10 000 MW cutoff membrane, Millipore), and the buffer was changed to PBE (55 mM phosphate, pH 7.4, 150 mM NaCl, 5 mM EDTA). After the products were mixed to incubate overnight at 4 °C and the unreacted DNA was removed by ultrafiltration (100 000 MW cutoff membrane, Millipore), the Ab-DNA was obtained. By measuring the UV−vis absorbance of Ab-DNA at 260 and 280 nm,[34] around five DNA strands were present on each Ab.

Measurement Procedure. The detection was performed by mixing 100 μg of MSN with 10 μL of 10× NEB buffer 4, 5 μL of 6 μM Ab1-DNA1 and Ab2-DNA2, 10 μL of 10 U Nt.BbvCI, 10 μL of various concentrations of PSA or serum sample obtained from a patient with prostate cancer, and ultrapure water to a total volume of 100 μL. After incubation at 37 °C for 50 min, the reaction solution was mixed with 100 μL of 0.1 M PBS, and 50 μL of the resulting solution was dropped onto the screen-printed electrode for electrochemical detection, which could adequately cover the electrode working area. Differential pulse voltammetry (DPV) from −500 to −100 mV (vs Ag/AgCl) with a pulse amplitude of 50 mV and a pulse width of 200 ms was performed to record the electrochemical response.

Polyacrylamide Gel Electrophoresis (PAGE) Analysis. An 8% native polyacrylamide gel was prepared using 1× TBE buffer. The loading sample was the mixture of 14 μL of DNA or DNA and Nt.BbvCI sample, 3 μL of 6× loading buffer, and 3 μL of UltraPowerTM dye and kept for 3 min so that the dye could integrate with DNA completely. Then the loading sample was injected into polyacrylamide hydrogel. The gel electrophoresis was run at 90 V for 60 min. The resulting board was illuminated with UV light and scanned with a Molecular Imager Gel Doc XR.

RESULTS AND DISCUSSION

Characterization of MSN. The morphology of MS nanoparticles was characterized by TEM (Figure 1A), which showed a porous structure of the uniform MS nanoparticles with a diameter around 120 nm. The size of MS nanoparticles was verified by DLS measurement (Figure 1B). In addition, the DLS results also reflected the good dispersity of MS nanoparticles in aqueous medium, which was essential for biological application. The nitrogen adsorption−desorption isotherm of the MS nanoparticles showed an average pore diameter of 2.5 nm (Figure 1C), which was in agreement with the porosity reflected by the TEM image. The total pore volume and total specific surface of MS nanoparticles were calculated to be 0.78 cm^3 g^{-1} and 862.5 m^2 g^{-1} by using the

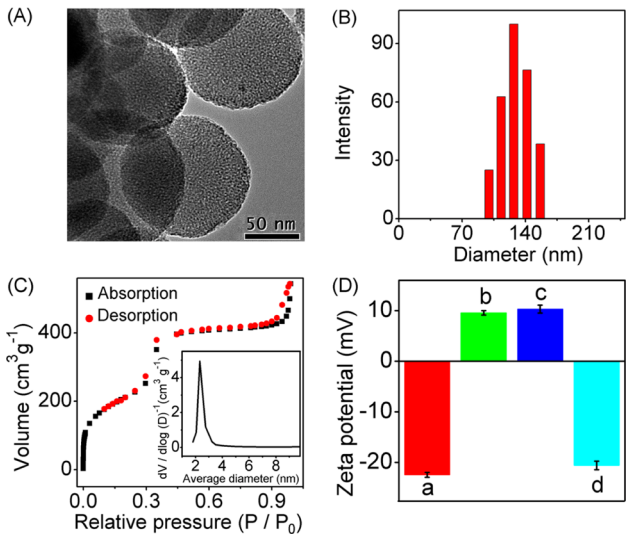

Figure 1. (A) TEM image, (B) DLS characterization, and (C) nitrogen adsorption−desorption isotherm of MS nanoparticles. Inset in C: pore size distribution. (D) Zeta-potential analysis of MS nanoparticles (a), amine-functionalized MS nanoparticles (b), MB-MS nanoparticles (c), and MSN (d).

dx.doi.org/10.1021/ac5012377 | Anal. Chem. 2014, 86, 7494−7499

BJH and BET model on the adsorption branch of the isotherm, respectively.

Zeta-potential analysis was used to characterize the preparation of MSN (Figure 1D). After functionalization with APTES, the MS nanoparticles became positively charged,[35,36] indicating that the amine groups were successfully functionalized on the surface of MS nanoparticles (column b). The entrapment of MB slightly increased the positive charge of the MS nanoparticle (column c). The positively charged amine-functionalized MS nanoparticles were beneficial for electrostatic adsorption of the negatively charged DNA (DNA3), resulting in a negatively charged MSN (column d). This result indicated the successful attachment of DNA3 on the surface of MS nanoparticles. The amount of DNA3 attached on MSN was determined to be 0.0362 mmol per gram of MS nanoparticles.

Feasibility of Proximity Hybridization Regulated DNA Biogate. The feasibility of the biogate was demonstrated with a control MSN sealed with DNA3′. After the control MSN was dispersed in 1× NEB buffer 4 for 50 min, the supernatant solution showed very weak fluorescence of both AMCA and MB (Figure 2, curve a), indicating that DNA3′ could tightly

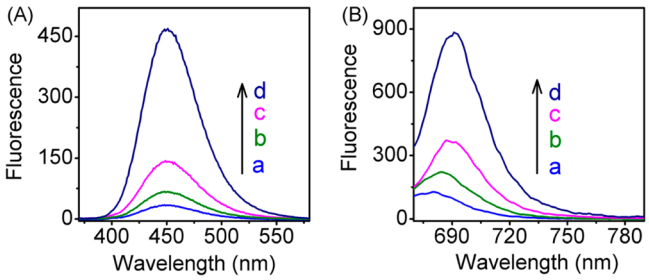

Figure 2. Fluorescence spectra of the supernatant solutions for (A) AMCA at λ_{ex} = 353 nm and (B) MB at λ_{ex} = 660 nm after incubating MSN with (a) 1× NEB buffer 4, (b) 1× NEB buffer 4 containing 0.3 μM Ab1-DNA1 and Ab2-DNA2 and 1 U Nt.BbvCI, (c) 1× NEB buffer 4 containing 0.3 μM Ab1-DNA1 and Ab2-DNA2 and 10 ng mL^{-1} PSA, and (d) 1× NEB buffer 4 containing 0.3 μM Ab1-DNA1 and Ab2-DNA2, 10 ng mL^{-1} PSA, and 1 U Nt.BbvCI.

wrap on the surface of MSN and the prepared MSN processed good stability. After the MSN was incubated with a mixture of Ab1-DNA1, Ab2-DNA2, and Nt.BbvCI for 50 min, the fluorescence intensity of the supernatant solution showed weak increase, which was attributed to the slight self-hybridization between DNA1 and DNA2 to produce the DNA strand complementary to DNA3′, and led to the detachment of some DNA3′ and release of MB (Figure 2, curve b). In the presence of 10 ng mL^{-1} of PSA, the incubation of control MSN with the mixture for the same time led to much stronger fluorescence intensity of both AMCA and MB (Figure 2, curve d), which reflected the simultaneous recognition of the target protein PSA by Ab1-DNA1 and Ab2-DNA2 to form proximate complex and lead to the dissociation of DNA3′ from the MSN surface by the hybridization of proximate complex with DNA3′, which opened the DNA "biogate". The fluorescence signals of both AMCA and MB were much higher than those in the absence of Nt.BbvCI (Figure 2, curve c), exhibiting the great amplification by Nt.BbvCI-based in situ enzymatic recycling.

The feasibility of proximity hybridization regulated DNA biogate was also confirmed by DPV detection (Figure S1, Supporting Information). Very weak DPV response was observed by incubating MSN in 1× NEB buffer 4 in the presence or absence of PSA (curves a and b). Upon addition of Ab-DNAs and Nt.BbvCI in the mixture of 1× NEB buffer 4 and MSN, the DPV peak current increased slightly, which was attributed to the slight self-hybridization between DNA1 and DNA2 (curve c). The similar DPV response was observed after Ab-DNAs, Nt.BbvCI, and MSN were added in blood serum from a healthy control (curve d), indicating that the complex components in serum did not induce the opening of DNA biogate and the release of MB from MSN. However, the presence of PSA led to a big increase of DPV response (curve f), suggesting the target-induced proximity hybridization and regulated DNA biogate. The DPV response was much higher than that in the absence of Nt.BbvCI (curve e), which confirmed the Nt.BbvCI-based in situ enzymatic amplification.

The DPV responses after incubating MSN with different components and pH values of buffer solutions containing 0.3 μM Ab-DNAs and 1 U Nt.BbvCI at different temperatures were examined (Figure S2, Supporting Information). All of the responses were similar to the background signal when incubating MSN in 1× NEB buffer 4 containing 0.3 μM Ab-DNAs and 1 U Nt.BbvCI, indicating that the DNA biogate on MSN was tight, and no release of MB was observed in the absence of target PSA.

Optimization of Detection Conditions. As the electrochemical signal resulted from the oxidation of released MB on a printed carbon electrode, the amount of MB in the mesopores, which depended on its concentration used for preparation of MSN, was first optimized. With increasing concentration of MB from 5 to 40 mg mL^{-1}, the DPV signal of the released MB increased and trended to plateau at 30 mg mL^{-1} (Figure 3A). So, 30 mg mL^{-1} of MB was chosen for the preparation of MSN.

The proposed immunoassay method employed an in situ enzymatic recycling for amplifying the electrochemical signal

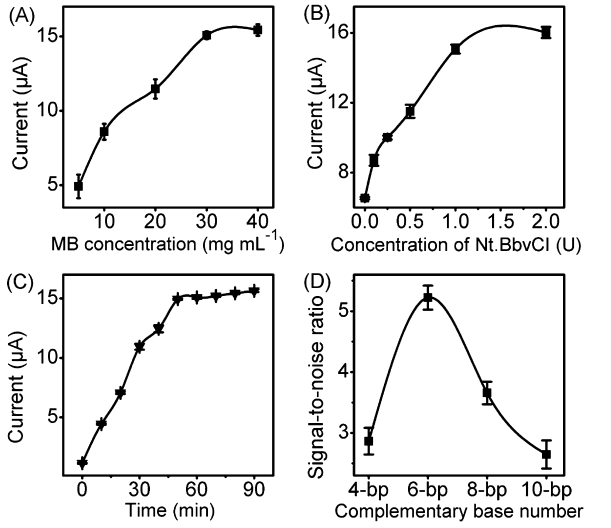

Figure 3. Effects of (A) MB concentration for preparation of MSN, (B) Nt.BbvCI concentration, (C) reaction time on oxidation peak current of released MB in the presence of 0.3 μM Ab1-DNA1 and Ab2-DNA2, 1 U Nt.BbvCI, and 20 ng mL^{-1} PSA, and (D) dependence of signal-to-noise ratio on complementary base number between DNA1 and DNA2′ at 0.3 μM DNA1 and DNA2′, 1 U Nt.BbvCI, and 10 nM ref DNA. In each optimization experiment, other parameters were their optimized values. Error bars represent standard deviations of three parallel experiments.

dx.doi.org/10.1021/ac5012377 | Anal. Chem. 2014, 86, 7494−7499

and improving the detection sensitivity, thus the concentration of Nt.BbvCI was also optimized. The peak current of the released MB in the presence of variable amounts of Nt.BbvCI increased and reached a plateau at 1 U of the nicking endonuclease (Figure 3B). Therefore, 1 U of Nt.BbvCI was used for the subsequent experiments, at which the peak current of the released MB was 2.3 times that in the absence of Nt.BbvCI, indicating the obvious signal amplification.

The reaction time was another important parameter affecting the analytical performance. It was clear that the current response increased with the increase of reaction time and tended to a maximum value at 50 min (Figure 3C). Hence, the optimum reaction time in this work was 50 min.

The opening of the biogate depended on the number of complementary bases between DNA1 and DNA2. In order to simplify the optimization of complementary base number, an 80 nucleotide DNA loop and DNA2′ without an −SH group were used to mimic the formation of the proximate complex.[28] The signal-to-noise ratios using DNA2′ with 4, 6, 8, and 10 bases complementary to DNA1 for proximity hybridization are shown in Figure 3D. In the presence of 10 nM ref DNA, the signal-to-noise ratio increased with the increasing number of complementary bases from 4 to 6 and then decreased from 6 to 10, indicating that DNA2 with a low number of bases complementary to DNA1 could not form the proximate complex, while DNA2 with a high number of bases could hybridize with DNA1 without the help of the proximate effect to produce a large background. According to the maximum signal-to-noise ratio, DNA2 with 6 bases complementary to DNA1 was chosen for the subsequent experiments.

The proximity hybridization of the optimized strands was further verified by PAGE analysis (Figure S3, Supporting Information). The mixture of DNA1, DNA2′, and DNA3 (lane 4) showed two bands at the same positions as DNA3 (lane 2) and DNA1 (lane 3), indicating that no hybridization among DNA1, DNA2′, and DNA3 occurred. When ref DNA was added to the mixture, a new band at ∼200 bp was observed, demonstrating the hybridization among DNA1, DNA2′, DNA3, and ref DNA and the formation of DNA1/ref DNA/DNA2′/DNA3 (lane 6). After Nt.BbvCI was added to this mixture, a new band occurred around 180 bp (lane 7), which was at the same position as the proximate complex formed in the mixture of DNA1, DNA2′, and ref DNA (lane 5), and could be attributed to the cleavage of DNA3 from DNA1/ref DNA/DNA2′/DNA3.

Assay Performance. The analytical performance of the homogeneous electrochemical immunoassay was characterized under optimal experimental conditions. As shown in Figure 4A, with the increasing PSA concentration, the oxidation peak current of MB increased correspondingly. It linearly depended on the logarithm of PSA concentration in the range of 0.002 to 100 ng mL^{-1} with a correlation coefficient of 0.9998 (Figure 4B). The detection limit corresponding to a signal-to-noise ratio of 3σ was 1.3 pg mL^{-1}, which was much lower than that of DNA displacement-based fluorescent assays.[30,31] The detection limit of pg mL^{-1} level with a detectable concentration range of 0.002 to 100 ng mL^{-1} was comparable to a commercial electrochemiluminescent analyzer (Elecsys 2010, Roche) with the detection range of 0.003−100 ng mL^{-1}, other electrochemical proximity assays,[28,29,33] and heterogeneous electrochemical immunoassays using nanomaterials for signal amplification.[37,38] In comparison with the detection limit of 6 pg mL^{-1} for a small molecule target,[25] the detection limit of 1.3 pg mL^{-1} for a protein showed much higher sensitivity. This could be attributed to the more sensitive DNA biogate than antibody-conjugated MSN and the nicking endonuclease-involved signal amplification.

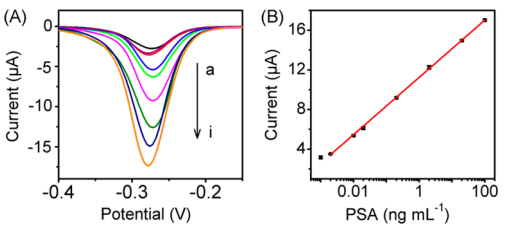

Figure 4. (A) DPV responses of homogeneous electrochemical immunoassay of PSA at 0, 0.001, 0.002, 0.01, 0.02, 0.2, 2, 20, and 100 ng mL^{-1} (from a to i), and (B) calibration curve. Error bars represent standard deviations of three parallel experiments.

The selectivity of the proposed immunoassay method was evaluated by comparing the peak current values of released MB in different solutions. Using carcinoembryonic antigen (CEA) as an interfering protein, it showed a response similar to the blank value, and the mixture of PSA and CEA showed a response similar to that of target PSA at the same concentration (Figure 5), indicating negligible response and interference of CEA with the detection of PSA. Overall, the high sensitivity, wide detection range, easy operation, and good selectivity of the proposed immunoassay indicated its great potential in point-of-care testing.

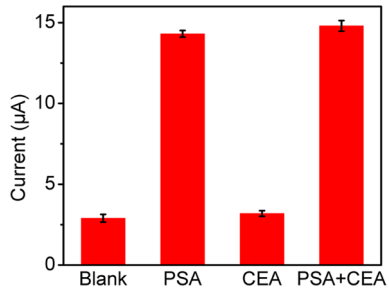

Figure 5. Oxidation peak current of released MB for blank control, 10 ng mL^{-1} PSA, 10 ng mL^{-1} CEA, and the mixture of 10 ng mL^{-1} CEA and PSA.

Real Sample Analysis. To evaluate the analytical reliability and application potential of the proposed method, it was used to detect PSA in clinical serum samples, and the assay results were compared with the reference values from the commercial electrochemiluminescent testing. The results shown in Table 1 showed an acceptable agreement with relative errors of less than 6.59%, indicating good accuracy of the proposed method for the detection of clinical samples.

CONCLUSION

This work presents a homogeneous electrochemical immunoassay method for convenient detection of protein biomarkers. This method uses a newly designed proximity hybridization regulated DNA biogate along with an in situ enzymatic recycling binding of the proximate complex to achieve high selectivity and high sensitivity. The target-induced proximity hybridization produces a DNA sequence complementary with the DNA strand attached on MSN and thus opens the DNA

dx.doi.org/10.1021/ac5012377 | Anal. Chem. 2014, 86, 7494−7499

Table 1. Assay Results of Clinical Serum Samples Using the Proposed and Reference Methods

sample no.	proposed method (ng mL^{-1})	reference method[a] (ng mL^{-1})	relative error (%)
1	0.52	0.51	1.96
2	18.4	19.7	−6.59
3	94.0	99.2	−5.24
4	5.27	5.14	2.53

[a]The reference levels were detected with an automated electrochemiluminescent analyzer (Elecsys 2010, Roche).

biogate to release the electroactive MB. Using PSA as a model target, the proposed assay shows a wide detection range, low limit of detection, and acceptable accuracy. The detection can be performed with single step, and this methodology can conveniently be extended to detect a wide range of analytes with available affinity ligands to form the proximate complex and thus possesses great potential for point-of-care testing.

■ ASSOCIATED CONTENT

Ⓢ Supporting Information

Additional information as noted in text. This material is available free of charge via the Internet at http://pubs.acs.org.

■ AUTHOR INFORMATION

Corresponding Author

*Phone/fax: +86-25-83593593. E-mail: hxju@nju.edu.cn.

Author Contributions

§K.R. and J.W. contributed equally to this work.

Notes

The authors declare no competing financial interest.

■ ACKNOWLEDGMENTS

We gratefully acknowledge the National Basic Research Program (2010CB732400), National Natural Science Foundation of China (21075055, 21135002, 21121091, and 21105046), Ph.D. Fund for Young Teachers (20110091120012), the Leading Medical Talents Program from Department of Health of Jiangsu Province, and Science Foundation of Jiangsu (BL2013036).

■ REFERENCES

(1) Choi, Y. E.; Kwak, J. W.; Park, J. W. *Sensors* **2010**, *10*, 428−455.
(2) Wang, J.; Liu, G.; Jan, M. R. *J. Am. Chem. Soc.* **2004**, *126*, 3010−3011.
(3) Lai, G. S.; Yan, F.; Ju, H. X. *Anal. Chem.* **2009**, *81*, 9730−9736.
(4) Mani, V.; Chikkaveeraiah, B. V.; Patel, V.; Gutkind, J. S.; Rusling, J. F. *ACS Nano* **2009**, *3*, 585−594.
(5) Munge, B. S.; Coffey, A. L.; Doucette, J. M.; Somba, B. K.; Malhotra, R.; Patel, V.; Gutkind, J. S.; Rusling, J. F. *Angew. Chem., Int. Ed.* **2011**, *50*, 7915−7918.
(6) Tang, D.; Yuan, R.; Chai, Y. *Anal. Chem.* **2008**, *80*, 1582−1588.
(7) Liu, G.; Wang, J.; Kim, J.; Jan, M. R.; Collins, G. E. *Anal. Chem.* **2004**, *76*, 7126−7130.
(8) Rusling, J. F. *Anal. Chem.* **2013**, *85*, 5304−5310.
(9) Xie, C.; Xu, F. G.; Huang, X. Y.; Dong, C. Q.; Ren, J. C. *J. Am. Chem. Soc.* **2009**, *131*, 12763−12770.
(10) Tachi, T.; Kaji, N.; Tokeshi, M.; Baba, Y. *Lab Chip* **2009**, *9*, 966−971.
(11) Geißler, D.; Stufler, S.; Löhmannsröben, H. G.; Hildebrandt, N. *J. Am. Chem. Soc.* **2013**, *135*, 1102−1109.
(12) Zhou, C. H.; Zhao, J. Y.; Pang, D. W.; Zhang, Z. L. *Anal. Chem.* **2014**, *86*, 2752−2759.
(13) Vivero-Escoto, J. L.; Slowing, I. I.; Trewyn, B. G.; Lin, V. S.-Y. *Small* **2010**, *6*, 1952−1967.
(14) Casasus, R.; Climent, E.; Marcos, M. D.; Martínez-Manez, R.; Sancenon, F.; Soto, J.; Amoros, P.; Cano, J.; Ruiz, E. *J. Am. Chem. Soc.* **2008**, *130*, 1903−1917.
(15) Aznar, E.; Marcos, M. D.; Martínez-Manez, R.; Sancenon, F.; Soto, J.; Amoros, P.; Guillem, C. *J. Am. Chem. Soc.* **2009**, *131*, 6833−6843.
(16) Xue, M.; Zink, J. I. *J. Am. Chem. Soc.* **2013**, *135*, 17659−17662.
(17) Climent, E.; Martinez-Manez, R.; Sancenon, F.; Marcos, M. D.; Soto, J.; Maquieira, A.; Amoros, P. *Angew. Chem., Int. Ed.* **2010**, *49*, 7281−7283.
(18) Luo, Z.; Cai, K.; Hu, Y.; Zhao, L.; Liu, P.; Duan, L.; Yang, W. *Angew. Chem., Int. Ed.* **2011**, *50*, 640−643.
(19) Liu, R.; Zhao, X.; Wu, T.; Feng, P. *J. Am. Chem. Soc.* **2008**, *130*, 14418−14419.
(20) Schlossbauer, A.; Warncke, S.; Gramlich, P. M. E.; Kecht, J.; Manetto, A.; Carell, T.; Bein, T. *Angew. Chem., Int. Ed.* **2010**, *49*, 4734−4737.
(21) Park, C.; Kim, H.; Kim, S.; Kim, C. *J. Am. Chem. Soc.* **2009**, *131*, 16614−16615.
(22) Vivero-Escoto, J. L.; Slowing, I. I.; Wu, C. W.; Lin, V. S. Y. *J. Am. Chem. Soc.* **2009**, *131*, 3462−3463.
(23) Park, C.; Lee, K.; Kim, C. *Angew. Chem., Int. Ed.* **2009**, *48*, 1275−1278.
(24) Tang, D. P.; Liu, B. Q.; Niessner, R.; Li, P. W.; Knop, D. *Anal. Chem.* **2013**, *85*, 10589−10596.
(25) Zhang, B.; Liu, B. Q.; Liao, J. Y.; Chen, G. N.; Tang, D. P. *Anal. Chem.* **2013**, *85*, 9245−9252.
(26) Zhang, Z.; Balogh, D.; Wang, F.; Willner, I. *J. Am. Chem. Soc.* **2013**, *135*, 1934−1940.
(27) Qian, R. C.; Ding, L.; Ju, H. X. *J. Am. Chem. Soc.* **2013**, *135*, 13282−13285.
(28) Hu, J. M.; Wang, T. Y.; Kim, J.; Shannon, C.; Easle, C. J. *J. Am. Chem. Soc.* **2012**, *134*, 7066−7072.
(29) Zhang, Y. L.; Huang, Y.; Jiang, J. H.; Shen, G. L.; Yu, R. Q. *J. Am. Chem. Soc.* **2007**, *129*, 15448−15449.
(30) Li, F.; Lin, Y. W.; Le, X. C. *Anal. Chem.* **2013**, *85*, 10835−10841.
(31) Li, F.; Zhang, H.; Lai, C.; Li, X. F.; Le, X. C. *Angew. Chem., Int. Ed.* **2012**, *51*, 9317−9320.
(32) Wu, S. S.; Huang, X.; Du, X. Z. *Angew. Chem., Int. Ed.* **2013**, *52*, 1−6.
(33) Ren, K. W.; Wu, J.; Yan, F.; Ju, H. X. *Sci. Rep.* **2014**, *4*, 4360−4365.
(34) Zhou, Z. J.; Xiang, Y.; Tong, A. J.; Lu, Y. *Anal. Chem.* **2014**, *86*, 3869−3875.
(35) Kim, Y. J.; Korkmaz, N.; Nam, C. H. *Interdiscip. Bio Cent.* **2012**, *9*, 1−7.
(36) Maaden, K. V. D.; Sliedregt, K.; Kros, A.; Jiskoot, W.; Bouwstra, J. *Langmuir* **2012**, *28*, 3403−3411.
(37) Yu, X.; Munge, B.; Patel, V.; Jensen, G.; Bhirde, A.; Gong, J. D.; Kim, S. N.; Gillespie, J.; Gutkind, J. S.; Papadimitrakopoulos, F.; Rusling, J. F. *J. Am. Chem. Soc.* **2006**, *128*, 11199−11205.
(38) Zani, A.; Laschi, S.; Mascini, M.; Marrazza, G. *Electroanalysis* **2011**, *23*, 91−99.